ACS NANO

www.acsnano.org

ARTICLE

Observation of Type-II Topological Nodal-Line Fermions in ZrSiSe

Minhao Zhao,[#] Zheng-Yang Zhuang,[#] Fan Wu,[#] Pengliang Leng,[#] Nesta Benno Joseph, Xiaoyi Xie, Mykhaylo Ozerov, Shanmei He, Yulin Chen, Awadhesh Narayan, Zhongkai Liu,* and Faxian Xiu*

Cite This: *ACS Nano* 2024, 18, 16684–16691

Read Online

ACCESS | Metrics & More | Article Recommendations | Supporting Information

ABSTRACT: Recently, there has been significant interest in topological nodal-line semimetals due to their linear energy dispersion with one-dimensional nodal lines or loops. These materials exhibit fascinating physical properties, such as drumhead surface states and 3D anisotropic nodal-line structures. Similar to Weyl semimetals, type-II nodal-line semimetals have two crossing bands that are both electron-like or hole-like along a certain direction. However, the direct observation of type-II nodal-line Fermions has been challenging due to the lack of suitable material platforms and the low density of states. Here we present experimental evidence for the coexistence of both type-I and type-II nodal-line Fermions in ZrSiSe, which was obtained through magneto-optical and angle-resolved photoemission spectroscopy (ARPES) measurements. Our density functional theory calculations predict that the type-II nodal-line structure can be developed in the Z-R line of the first Brillouin zone based on the lattice constants of the grown single crystal. Indeed, ARPES measurements reveal the type-II nodal-line band structure. The extracted type-II Landau level transitions from magneto-optical measurements exhibit good agreement with the calculated type-II energy dispersion model based on the band structure. Our experimental results demonstrate that ZrSiSe possesses two types of nodal-line Fermions, distinguishing it from other ZrSiX (X = S, Te) materials and positioning it as an ideal platform for investigating type-II nodal-line semimetals.

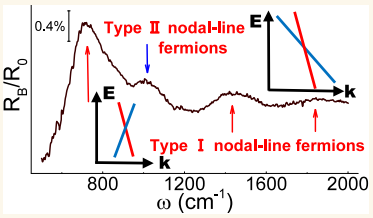

KEYWORDS: *nodal-line semimetal, magneto-optical spectrum, Landau level transition, band structure, two types of nodal-line structures*

Soon after the proposal of type-II Weyl semimetals,[1] extensive experiments were conducted to identify potential candidates. Some materials have been confirmed as type-II Weyl semimetals, and their unique electromagnetic responses, such as Fermi arcs and the chiral anomaly, have been reported.[2−5] More recently, nodal-line semimetals have been predicted as a new class of topological materials with linear energy dispersion.[6,7] Unlike discrete band crossing points found in Dirac or Weyl semimetals, nodal-line semimetals exhibit a one-dimensional line or loop of band crossings.[6] Several topological nodal-line semimetals have been experimentally established, including $PbTaSe_2$,[8] $PtSn_4$,[9] $SrAs_3$,[10,11] and ZrSiX (X = S, Se, Te).[12,13] Similar to the band inversion structure in type-II Weyl semimetals, tilted lines or loops are also allowed in nodal-line semimetals, giving rise to a new class of materials called type-II nodal-line semimetals.[14,15] However, the experimental observation of type-II nodal-line Fermions remains challenging due to the lack of effective tools to investigate Fermi surfaces and Landau-level quantizations, as well as the absence of an ideal material platform with a robust type-II nodal-line band structure. Among the reported nodal-line semimetals, the ZrSiX family of materials has attracted significant attention due to the large energy window of the linear band dispersion in certain regions of the Brillouin zone.[16] The band structures of these materials have been extensively investigated through theoretical calculations and angle-resolved photoemission spectroscopy (ARPES) measurements.[12,16−22] While the physical properties of typical type-I nodal-line semimetals have been studied using various transport and optical measurements,[13,16,17,23−27] the band structure of ZrSiX near the Fermi energy in the Z-R range is predicted to exhibit the shape of a type-II nodal line, especially in the case of ZrSiSe.[16]

In this study, we present our findings on the coexistence of type-I and type-II nodal-line Fermions in ZrSiSe. To obtain high-quality ZrSiSe single crystals, we employed a two-step chemical vapor transport process that utilized I_2 as the transport agent. Surprisingly, the lattice constant c in our samples was found to be smaller than previously reported values. Our density functional theory (DFT) calculations revealed the presence of a clearly tilted type-II nodal line structure along the Z-R line, while the type-I nodal line

Received: February 2, 2024
Revised: May 31, 2024
Accepted: June 3, 2024
Published: June 17, 2024

https://doi.org/10.1021/acsnano.4c01633
ACS Nano 2024, 18, 16684−16691

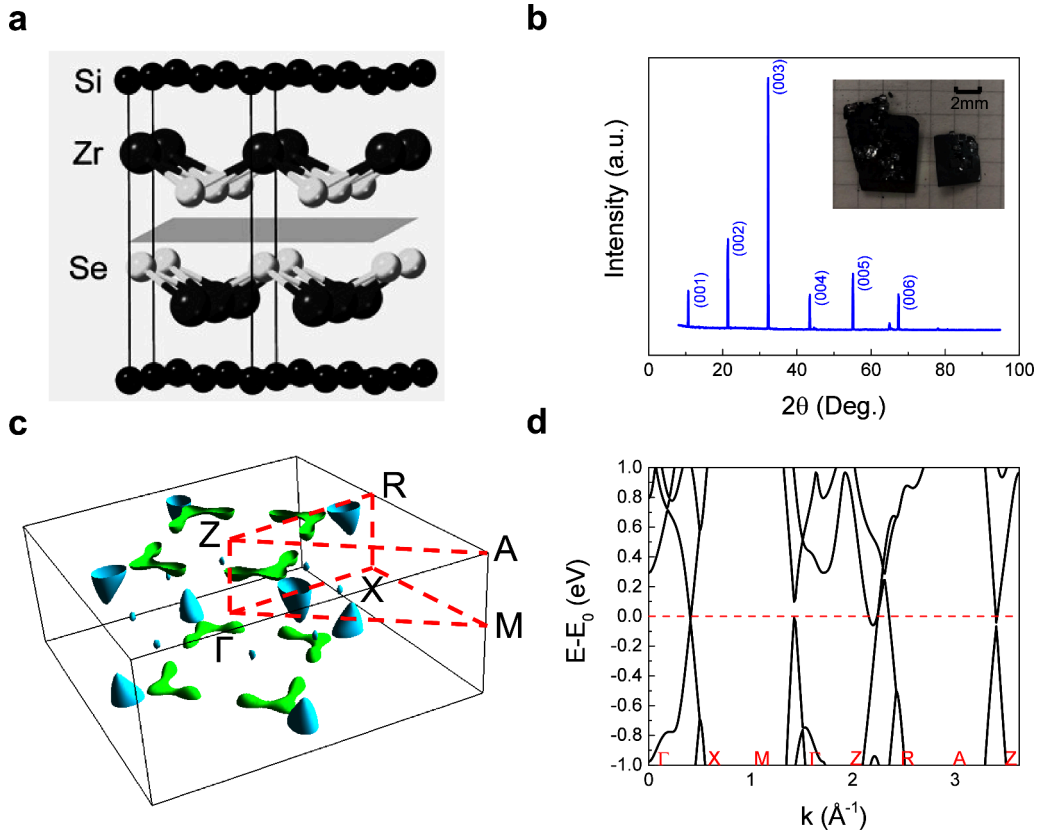

Figure 1. Crystal and band structure of ZrSiSe. a. Crystal structure of ZrSiSe. b. Single crystal XRD spectrum, showing the (001) crystal planes of single crystallinity of ZrSiSe. The inset shows a photo of the sample with a length of 2 mm. c. Calculated Fermi surface of ZrSiSe. d. Band structure of ZrSiSe. The red dashed line denotes its Fermi energy.

remained intact. To observe the existence of the type-II nodal-line band structure in ZrSiSe, we performed angle-resolved photoemission spectroscopy (ARPES) measurements. By analyzing the magneto-optical spectra, we obtained Landau level transitions originating from both types of nodal lines. The Landau level transitions corresponding to the type-I nodal-line Fermions were well-fitted with a gapped linear energy dispersion model, which is consistent with previous research findings.[27] On the other hand, the Landau level transitions associated with the type-II nodal-line Fermions were determined by comparing the spectra obtained from Faraday and Voigt geometries. By combining our DFT calculations and magneto-transport measurements, we established a low-energy Hamiltonian for the type-II nodal-line which can effectively capture the tilted structure. Intriguingly, our transport measurements provided evidence that the carriers along the Z-R line were active and dominated the transport behaviors. Furthermore, we found that other materials in the ZrSiX family lack the type-II nodal-line structure, and only Landau level transitions from the type-I nodal-line structure were observed in the magneto-optical measurements. Thus, our study demonstrates the coexistence of type-I and type-II nodal-line Fermions in the topological material ZrSiSe, characterized by specific lattice constants. Additionally, we show that magneto-optical measurements are effective in experimentally investigating complex topological systems.

RESULTS AND DISCUSSION

The crystal structure of ZrSiX can be described as a typical layered compound consisting of quintuple layers of X-Zr-Si-Zr-X. ZrSiX adopts a PbFCl-type crystal structure with the space group *P*4/*nmm*, as illustrated in Figure 1a. In this structure, each quintuple layer is centered around the Si layer which forms a tetrahedral coordination with four Zr atoms. The X atoms are positioned on the two sides of each quintuple layer and interact weakly with the neighboring layers through van der Waals forces.[13,28] High-quality single-crystal ZrSiSe was grown using a chemical vapor transport method. A stoichiometric mixture of Zr, Si, and Se powders was sealed in a quartz tube, and iodine was used as a transport agent (2 mg/cm^3). Plate-like single crystals with metallic lusters were obtained by conducting vapor transport growth with a temperature gradient from 950 to 850 °C.[13] The inset of Figure 1b shows the 3 × 3 mm^2 samples. The composition and structure of the crystals were examined using an Energy-dispersive X-ray spectrometer and X-ray diffractometer, respectively. Figure 1b displays a representative X-ray diffraction pattern obtained from a single crystal sample, revealing preferred orientation along the (00l) and (110) planes. Based on the diffraction peaks, refined lattice parameters were determined as $a = b = 3.66$ Å and $c = 8.47$ Å. It is worth noting that our experimental lattice parameter differs from the reported value of $c = 8.676$ Å[29]. Our sample has a relatively lower c constant. The small lattice parameter c has been reported in earlier studies where the growth methods are not uncommon.[29] The lattice parameter c has generally been observed to be similarly lower, at around 8.3 Å, and the type-I nodal-line structure has not been impacted.[13] The smaller lattice parameter has been identified in the actual sample growth. Our growth process is not unique but the

https://doi.org/10.1021/acsnano.4c01633
ACS Nano 2024, 18, 16684−16691

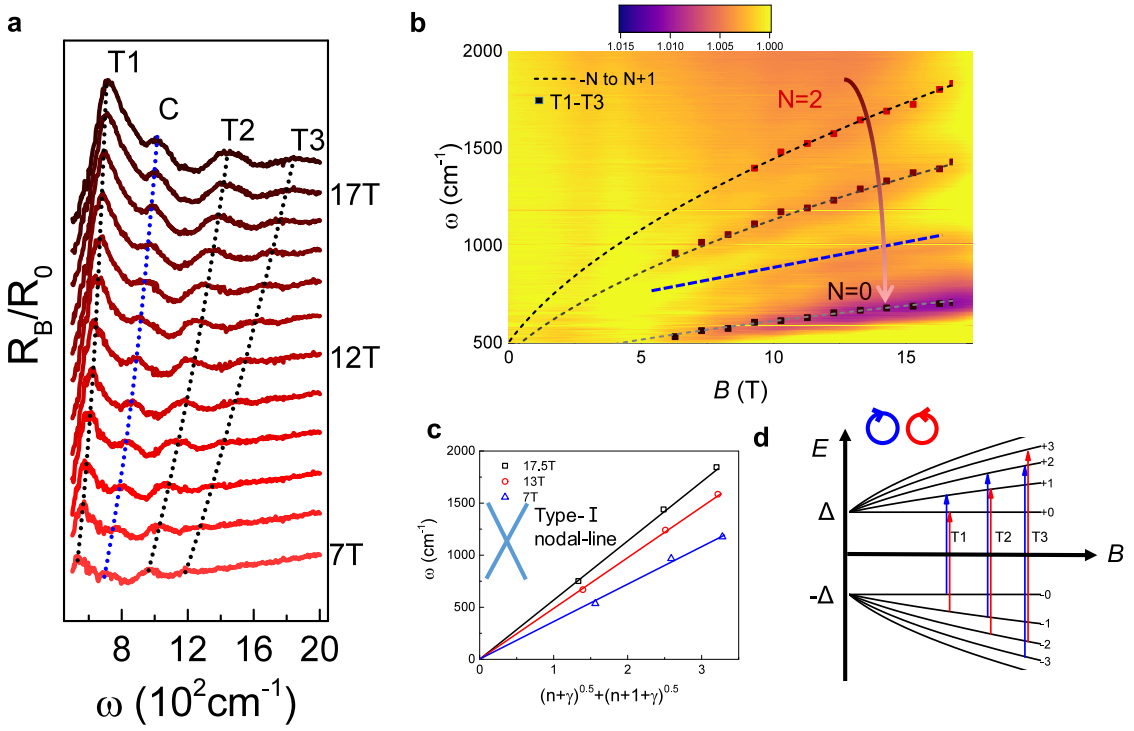

Figure 2. Type-I Landau level transitions of ZrSiSe. a. Magneto-optical spectra of ZrSiSe obtained under Faraday geometry, showing two types of peaks classified as C-type and T-type transitions. b. A false-color plot of relative magneto-reflectance spectra. The black dashed lines are the fitting curves of type-I nodal line Landau level transitions. The blue dashed line denotes the position of the C-type transition. c. Landau fan diagrams for the type-I nodal line in ZrSiSe under varying magnetic fields. The labels indicate the experimental transition energy and Landau level index from −0 → 1 to −2 → 3 with increasing incident energy under different magnetic fields. The solid lines serve as guidelines, confirming the presence of type-I nodal-line Fermions and the assignment of transition indices using the fitted Fermi velocity. d. Schematic Landau level spectrum of the type-I nodal line in ZrSiSe. The blue and red arrows denote the inter-Landau-level transitions with opposite circular polarizations.

resulting lattice constants are critical to the presence of type II nodal-line structure.

Based on the experimentally obtained lattice constants of ZrSiSe, we conducted first-principles calculations to investigate the Fermi surface and band structure (see Methods for details). The calculated 3D Fermi surface is presented in Figure 1c. The type- I nodal-line structure has been confirmed in the A-Z direction. And in the Z-R line, we observe two pockets, one with holes and the other with electrons, intersecting and forming a type-II nodal line structure. To further illustrate the electronic properties, Figure 1d displays the band structure with spin−orbit coupling (SOC) along the high-symmetry lines. The position of the Fermi energy is indicated by the red dotted line. Notably, we observe a series of Dirac-type bands with linear dispersion near the Fermi energy, resulting in a type-I nodal-line structure along the Γ-X direction in the first Brillouin zone. Additionally, there is a band inversion along the Z-R line, leading to the formation of a type-II nodal-line structure. Therefore, our theoretical analysis predicts the coexistence of the type-I nodal line along Γ-X and the type-II nodal line along Z-R in ZrSiSe.

In order to investigate the energy dispersion of the two types of nodal-line Fermions, we employed magneto-optical measurements as an effective tool to identify the Landau level transitions around the Fermi energy in ZrSiSe. The magneto-optical spectra on the (001) surface under Faraday geometry are presented in Figure 2a. For more experimental details, please refer to the Methods section. We observed four distinct reflection features, which we classify into two types of Landau-level transitions denoted as C-type and T-type, respectively. Previous studies on magneto-optical properties[27] suggest that a gapped massive nodal-line dispersion model can be applied to fit the T-type transitions. The Landau level quantization is described by[30] $E_{\pm n} = \pm\sqrt{2e\hbar|n|Bv^2\cos(\phi) + (\Delta/2)^2}$, where n is the Landau level index, v is the Fermi velocity, ϕ is the angle between the nodal-line direction and the magnetic field direction. The selection rule for Landau level transitions is given by $\Delta n = |n_i| - |n_f| = \pm 1$,[31,32] where n_i and n_f are the Landau level index of the initial and final states, respectively. The dashed curves shown in Figure 2b represent the best-fitting results obtained using the gapped model with assigned transition indices. The Fermi velocity is extracted to be $v_F = 3.72 \times 10^5$ m/s. The fitted band gap is found to be $\Delta \sim 40$ meV, which is consistent with previous studies.[27] Based on these fitting results, the T-type Landau level transitions can be classified as type-I nodal-line Landau level transitions. To further validate the fitted Landau indices and the accuracy of the fitting for the T-type transitions, we summarize the Landau indices and the transition energies in Figure 2c. The parameter γ denotes a constant which is calculated by the function $\left(\frac{\Delta}{2}\right)^2/(2e\hbar Bv^2\cos(\phi))$. γ changes with the magnetic field. We confirm that the T-type transitions originate from type-I nodal-line Fermions and also exclude the possibility of the conventional semiconductor origin. Moreover, the corresponding Landau indices include not only −N → N+1 but also −(N

https://doi.org/10.1021/acsnano.4c01633
ACS Nano 2024, 18, 16684−16691

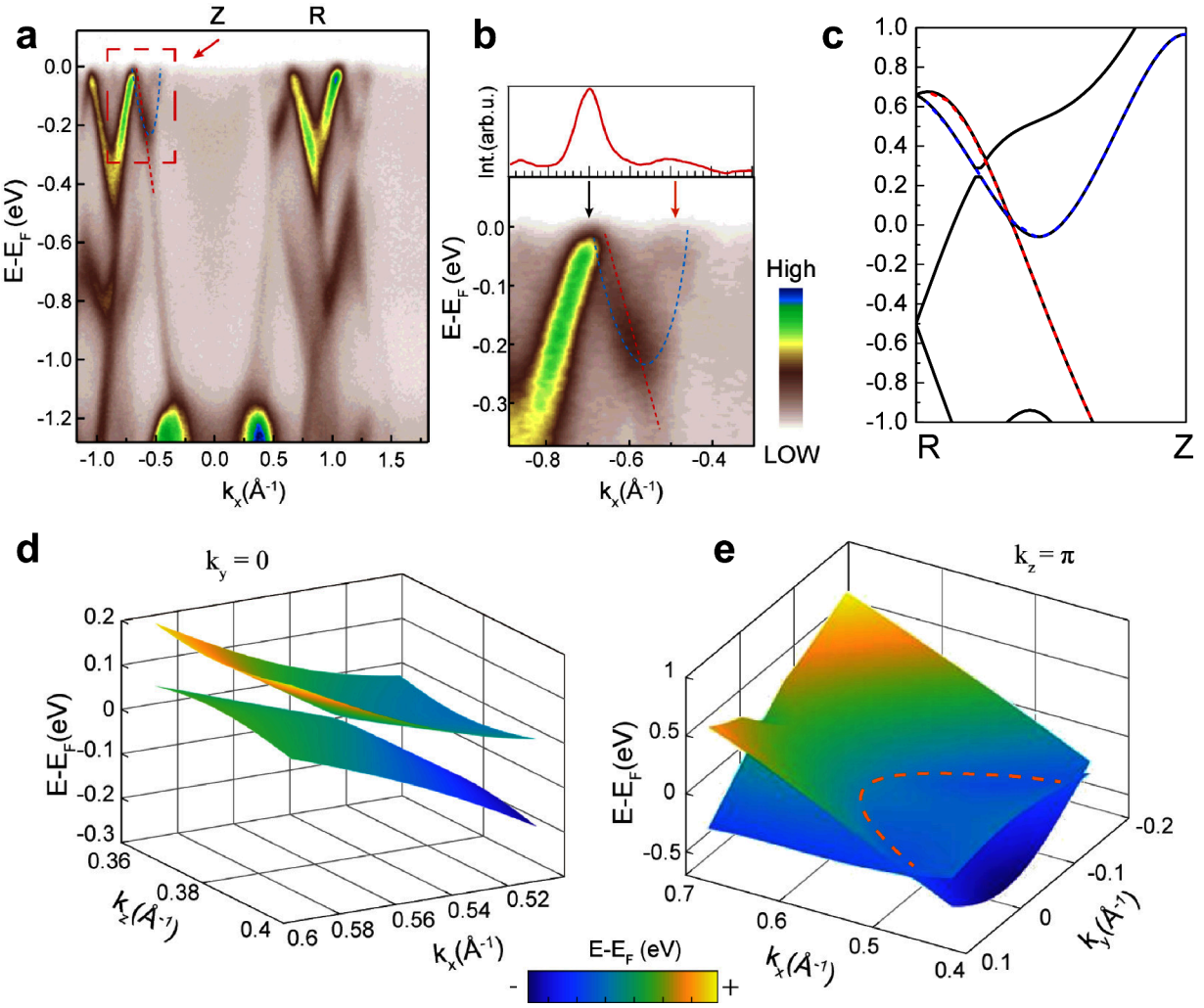

Figure 3. Type-II nodal-line band structure in ZrSiSe. a. The band dispersion along the Z-R direction was measured at 15K using ARPES with 114 eV photon beazm. b. A zoomed-in view of the red-boxed area on the left. The red curve is the momentum distribution curve (MDC) close to Fermi energy in the right panel. The yellow and orange dashed lines stand for electron pocket and hole pocket, respectively. c. DFT calculated band structure in the Z-R range. The red and blue lines correspond to the orange and yellow lines in panel a respectively. d. Band dispersion of k_x-k_z plane at k_z = 0. e. Band dispersion of of k_x-k_z plane at $k_z = \pi$.

+1) → N. The results of all T-type Landau level transitions and their energy dispersion are presented in Figure 2d. It is worth noting that the blue and red lines represent the Landau level transitions that are active in the σ+ and σ- polarizations of the incoming light, respectively.[33−35] Furthermore, we found that the C-type transition cannot be fitted using the gapped model for type-I nodal-line Fermions, indicating that this transition is arising from another band.

To identify the proposed type-II nodal-line band structure, we performed high-resolution ARPES measurement on ZrSiSe. Despite ZrSiSe being extensively studied as a type-I nodal-line semimetal, our study not only confirms the existence of type-I nodal-line structure but also finds the type-II nodal-line structure in the Z plane. The small difference in the lattice constants does not change the type-I nodal-line structure, so we can observe similar behavior of the type-I nodal-line structure. Based on our DFT calculation, the lattice constants of our sample result in the formation of the type-II nodal-line structure. Comprehensive photon energy-dependent measurement was conducted to precisely locate the $k_z = \pi/2$ plane in the Brillouin Zone (BZ) (see Supplementary Materials V), and *in situ* Rb surface dosing was used to elevate the Fermi level of the pristine sample to better visualize the nodal-line structure (details can be found in Supplementary Materials V). Our main result is depicted in Figure 3a, where the band dispersion along the Z-R direction is illustrated. The electron and hole pockets are marked by the yellow and orange dashed lines, respectively. A type-II nodal line is formed, where these two bands intersect. This intersection can be better visualized from the zoomed-in plot as shown in Figure 3b. Our experimental result is in line with the calculated bandstructure along the Z-R direction (Figure 3c) where tilted bands intersect and form the predicted type-II nodal-line structure. Based on the experimentally confirmed lattice constants, our DFT calculation and ARPES experiment have revealed the existence of type-II nodal-line structure. This provides a foundation to further explore the behavior of the type-II nodal-line Fermions. Figure 3d shows the band dispersion of the k_x-k_z plane at k_z = 0. It can be clearly seen that the band intersection only exists at the Z point in the k_z direction. In Figure 3e, the nodal line is marked by an orange dotted line in Z plane ($k_z = \pi$), More detailed calculations and ARPES results are shown in Supplementary Materials V.

https://doi.org/10.1021/acsnano.4c01633
ACS Nano 2024, 18, 16684−16691

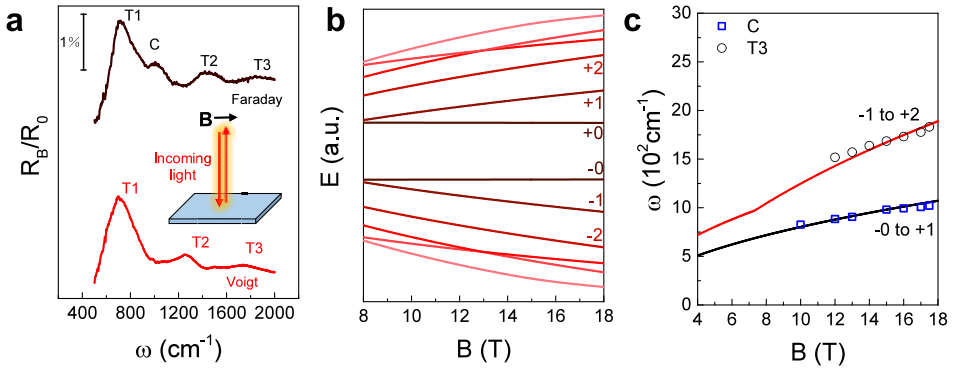

Figure 4. Type-II nodal line transition. a. Comparison of spectra under Faraday and Voigt geometries. The inset shows a schematic diagram of the Voigt geometry setup. b. The calculated energy spectrum of type-II nodal line Landau levels. c. Fitting result of C-type transition in the type-II nodal line model.

Based on the calculated band structure and the ARPES measurements, considering the tilt of the nodal line, the generic low-energy Hamiltonian near the nodal line can be expressed as follows:

$$H(\mathbf{q}) = \gamma(q_x^{\,2} - q_y^{\,2}) + \lambda(q_x^{\,2} + q_y^{\,2} - q_0^{\,2})\sigma_z + v_z q_z \sigma_x + \Delta\sigma_y$$

where Δ*is* introduced to control the size of the finite gap. The tilt is controlled by the ratio γ/λ, where γ and λ have the dimensions of the inverse of mass that describe the inclination. This generic low-energy Hamiltonian can describe both type-I dispersion ($\gamma/\lambda < 1$) and type-II dispersion ($\gamma/\lambda > 1$). However, as we have acquired very detailed band structure information near the type-II nodal line through DFT calculations and ARPES measurements, we will consider the following Hamiltonian, which can capture a broader range of the real band structure, to understand the magneto-optical spectra involving the type-II nodal line. To be specific, the Hamiltonian has the form

$$H(k) = \begin{pmatrix} \dfrac{\hbar^2(k_x - k_c)^2}{2m_c} + U_c & v_y\hbar k_y - iv_z\hbar k_z \\ v_y\hbar k_y + iv_z\hbar k_z & -\dfrac{\hbar^2(k_x - k_v)^2}{2m_v} + U_v \end{pmatrix}$$

where U_c and U_v reflect the energy offset between the band edge of the conduction and valence bands, k_c and k_v reflect the separation of the locations of conduction and valence band edges, and other parameters have the usual meaning as effective mass or velocity.

In the presence of a magnetic field, one can determine the Landau levels by replacing the momentum via the Landau ladder operators, i.e.,

$$\hbar k_x = \sqrt{\frac{\hbar eB}{2}}(a + a^\dagger), \qquad \hbar k_y = -i\sqrt{\frac{\hbar eB}{2}}(a - a^\dagger)$$

where $a(a^\dagger)$ refers to the lowering (raising) operator and satisfies $[a, a^\dagger] = 1$, and then diagonalizing the total Landau level Hamiltonian under the harmonic-oscillator basis. Further details are provided in Supplementary Materials III.

Now the energy dispersion mode can be induced to search for the origin of the C-type transition. To this end, we conducted magneto-transport measurements for ZrSiSe. The Hall effect signal was found to be weak, suggesting that holes and electrons contribute almost equally to the carrier population. This behavior is consistent with the Z-R band structure where the Fermi energy intersects both the conduction and valence bands, resulting in subequal hole and electron pockets. We analyzed the quantum oscillations and examined the Fermi surface (see Supplementary Materials II). The frequency of the oscillation corresponds to the pockets along the Z-R line, indicating that the carriers near the Fermi surface in the Z-R band are detectable. The transport behavior is dominated by the carriers along the Z-R line, implying that the density of states of the Fermions is sufficient for detection. In addition, magneto-optical measurements under Voigt geometry were performed to compare the C-type transition with T-type transitions. As shown in Figure 4a, only the C-type transition disappears when B⊥k_z. This observation suggests that the C-type transition arises from a different band structure compared to the T-type transitions. Combining the results from transport and magneto-optical measurements, it is likely that the Fermions near the Fermi surface in the Z-R range are responsible for the C-type transition. To verify this hypothesis, it is crucial to examine the energy dispersion mode of the Fermions in the Z-R range. Using the theoretically calculated Hamiltonian and fitting parameters of the band structures, we extracted the energy dispersion mode of type-II nodal-line Fermions in the Z-R range. The calculated energy spectrum of the Landau levels is presented in Figure 4b. The C-type transition energy agrees well with this model, with a Fermi velocity parameter v_{F1} = 6.5 × 10^5 m/s, which is close to the Fermi velocity v_{F2} = 6.42 × 10^5m/s extracted from the transport measurements (Figure 4c). The corresponding Landau index is −0 to +1 or −1 to +0. Additionally, to confirm our fitting result, the trace of another interband Landau level transition is found and has a good agreement with our theoretical type-II nodal-line model. As shown in Figure 4c, the T3 transition can be fitted in the type-II model. T3 transition can be detected under both Faraday and Voigt geometries which is different from the C-type transition. However, the calculated transition energy for −1 + 2 transition is highly consistent with the T3 transition. In this case, we can identify the T3 transition as −2 + 3 transition in the type-I nodal-line structure and −1 + 2 transition in the type-II nodal-line structure. The T3 transition has a good agreement with the two models. It also explains the reason why the noise of T3 transition is relatively high under low magnetic fields. The quality of the fitting and its consistency with the

https://doi.org/10.1021/acsnano.4c01633
ACS Nano 2024, 18, 16684−16691

transport measurements support the conclusion that the C-type transition originates from the type-II nodal-line Fermions in the Z-R range.

To further validate the origin of the C-type transition, we conducted investigations on other materials from the ZrSiX family with similar crystal structures as ZrSiSe. In addition to ZrSiSe, we performed magneto-optical measurements on ZrSiS to observe Landau level transitions. By comparing the spectra under Faraday and Voigt geometries, we found that the C-type Landau level transition does not exist in ZrSiS. Furthermore, based on the DFT calculations of the band structure of ZrSiS,[21] we determined that the tilted nodal-line structure is not formed within the Z-R range. The magneto-optical spectra and a detailed analysis can be found in the Supplementary Materials IV. By comparing the band structures of ZrSiSe and ZrSiS, we observed that the type-I nodal-line structures in both materials are similar and can be detected in magneto-optical measurements. However, the absence of the type-II nodal-line structure in ZrSiS results in the lack of a C-type Landau level transition. Regarding ZrSiTe from the ZrSiX family, we did not detect any signals in the magneto-optical measurements. This could be due to the low mobility of ZrSiTe, which prevents the Landau level transitions from occurring in the nodal-line Fermions. Additionally, the theoretically calculated band structure of ZrSiTe does not exhibit the type-II nodal-line structure. Furthermore, the energy dispersion of the C-type transition follows a $\sqrt{B}$-like dispersion mode, which is not observed in conventional semiconductor bands. After excluding the type-I nodal-line Fermions and conventional parabolic dispersive Fermions, we can conclude that the C-type Landau level transition originates from the Z-R band of ZrSiSe. The coexistence of type-I and type-II nodal-line Fermions is only observed in ZrSiSe, as summarized in Table1. These results confirm the coexistence of both types of nodal-line Fermions in ZrSiSe, and demonstrate that both types are experimentally detectable.

Table 1. Definition of Nodal Line Types in ZrSiX Materials

	Z-R band inversion	Type I	Type II
ZrSiS	×	√	×
ZrSie	√	√	√
ZrSTe	×	√	×

CONCLUSIONS

Since the proposal of nodal-line semimetals as a new quantum state in topological Dirac material systems, the experimental identification of type-II nodal-line semimetals has remained elusive. ZrSiSe, as the earliest candidate for a nodal-line semimetal, has provided evidence of type-I nodal-line Fermions through both transport and optical measurements. Through our band structure calculations, we have determined that the type-II nodal-line structure is developed in ZrSiSe due to the experimental lattice parameters. The existence of the type-II of nodal-line band structures is confirmed by ARPES measurements. Moreover, the T-type and C-type Landau level transitions extracted from magneto-optical measurements agree well with the type-I and type-II nodal-line models, respectively. By combining magneto-transport and magneto-optical measurements under different geometries, as well as comparing with other materials in the ZrSiX family, we have established that the density of states of type-II nodal-line Fermions in the Z-R line of ZrSiSe is sufficiently large. The C-type Landau level transition in ZrSiSe is classified as a −1 to +2 type-II nodal-line Landau level transition. The tilted nodal line structure only forms in ZrSiSe, and the type-II nodal-line Fermions can be experimentally observed. In the presence of an electromagnetic field, the type-II nodal-line structure indeed displays distinctive behaviors. We have presented that the C-type Landau level transitions in magneto-optical spectra are exclusive for the type-II nodal line semimetals under Faraday geometry. This is one of the emerging optical phenomena that is rooted in the type-II nodal-line band structure. In addition, there are other intriguing effects associated with the type-II band structure. For example, in type-II nodal line semimetals, the electron and hole pockets coexist at the energy near where the nodal line structure is located. Therefore, when the chemical potential is lying at that energy, the effects of Landau−Zener transitions between the electron and hole pockets are pronounced, leading to additional cyclotron orbits for electrons. This phenomenon is known as "magnetic breakdown", and can be viewed as a momentum space counterpart of Klein tunneling at a p−n junction. It can be observed through the periodicity of quantum oscillations in the measurement of de Haas-van Alphen effects. However, for type-I nodal line semimetals, Klein tunneling will not occur, since there is only one type of pocket at an energy.

Our theoretical and experimental results demonstrate that ZrSiSe serves as an excellent platform for studying the unique properties of type-II nodal-line Fermions and confirm the Landau energy dispersion mode associated with the type-II nodal-line structure.

METHODS

Broadband infrared reflection measurements were conducted using a Bruker 80 V Fourier-transform IR spectrometer in both the Voigt and Faraday configurations. The collimated infrared beam emitted from the spectrometer was directed into an evacuated beamline, where it was focused at the upper end of a brass light pipe fitted with a diamond window. Subsequently, the infrared beam was guided through the pipe to reach the sample region located within the 17.5 T vertical bore superconducting magnet. The sample was positioned between two confocal 90° off-axis parabolic mirrors, which were mounted at the base of the probe. The first mirror was responsible for focusing the IR radiation onto the sample, while the second mirror collimated the reflected radiation toward a short light pipe that housed a 4 K composite Si bolometer at its end. To control the incident IR light's polarization, a thin-film wire-grid polarizer was placed in front of the first mirror. The sample temperature was maintained at 5.5 K using a small amount of helium exchange gas. Magneto-transport measurements were carried out employing a physical property measurement system (PPMS) utilizing a standard Hall-bar geometry. Lock-in amplifiers were used for measuring the electrical signals. ARPES measurements were performed at beamline BL03U of Shanghai Synchrotron Radiation Facility (SSRF), China (photon energy $h\nu$ = 7−165 eV) and beamline 7 (MAESTRO) of the Advanced Light Source. The samples were cleaved *in situ* at 15 K (5.8 K) and measured in an ultrahigh vacuum with a base pressure of better than 5×10^{-11} (4×10^{-11}) mbar at SSRF (ALS). Data were obtained by a DA30 (R4000) electron analyzer at SSRF (ALS). The energy and momentum resolution were 10 meV (20 meV) and 0.2° (0.1°) at SSRF (ALS), respectively. Our first-principles calculations were carried out within the DFT framework as implemented in the QUANTUM ESPRESSO code.[36,37] A kinetic energy cutoff of 55 Ry was considered, using the ultrasoft pseudopotentials to describe the core electrons, including semiempirical Grimme's DFT-D2[38] correction for the van der Waals forces present in the system. We used the Perdew−Burke−Ernzerhof (PBE) form of the generalized

https://doi.org/10.1021/acsnano.4c01633
ACS Nano 2024, 18, 16684−16691

gradient approximation (GGA) for the exchange-correlation function,[39] including spin−orbit coupling (SOC) interactions. The Brillouin zone was sampled over a uniform Γ-centered k-mesh of 10 × 10 × 4.

ASSOCIATED CONTENT

Data Availability Statement

The data that support the plots within this paper and other findings of this study are available from the corresponding author upon reasonable request.

Supporting Information

The Supporting Information is available free of charge at https://pubs.acs.org/doi/10.1021/acsnano.4c01633.

Landau level transitions under Voigt geometry, transport measurements of ZrSiSe, physics of type II nodal-line dispersion, Landau level transitions in ZrSiS, ARPES measurement of ZrSiSe, and cyclotron resonance in ZrSiSe (PDF)

AUTHOR INFORMATION

Corresponding Authors

Faxian Xiu − *State Key Laboratory of Surface Physics and Department of Physics and Institute for Nanoelectronic Devices and Quantum Computing, Fudan University, Shanghai 200433, China; Shanghai Qi Zhi Institute, Shanghai 200232, China; Zhangjiang Fudan International Innovation Center, Fudan University, Shanghai 201210, China; Shanghai Research Center for Quantum Sciences, Shanghai 201315, China;* orcid.org/0000-0003-2860-0369; Email: faxian@fudan.edu.cn

Zhongkai Liu − *School of Physical Science and Technology, ShanghaiTech University, Shanghai 201210, China; Lingang Laboratory, Shanghai 200031, China;* orcid.org/0000-0003-3373-8039; Email: liuzhk@shanghaitech.edu.cn

Authors

Minhao Zhao − *State Key Laboratory of Surface Physics and Department of Physics, Fudan University, Shanghai 200433, China; Shanghai Qi Zhi Institute, Shanghai 200232, China*

Zheng-Yang Zhuang − *School of Physics, Sun Yat-Sen University, Guangzhou 510275, China;* orcid.org/0000-0001-5749-9656

Fan Wu − *School of Physical Science and Technology, ShanghaiTech University, Shanghai 201210, China; Lingang Laboratory, Shanghai 200031, China*

Pengliang Leng − *State Key Laboratory of Surface Physics and Department of Physics, Fudan University, Shanghai 200433, China; Shanghai Qi Zhi Institute, Shanghai 200232, China*

Nesta Benno Joseph − *Solid State and Structural Chemistry Unit, Indian Institute of Science, Bangalore 560012, India;* orcid.org/0000-0003-0538-0148

Xiaoyi Xie − *State Key Laboratory of Surface Physics and Department of Physics, Fudan University, Shanghai 200433, China; Shanghai Qi Zhi Institute, Shanghai 200232, China*

Mykhaylo Ozerov − *National High Magnetic Field Laboratory, Florida State University, Tallahassee, Florida 32310, United States;* orcid.org/0000-0002-5470-1158

Shanmei He − *Department of Physics, Clarendon Laboratory, University of Oxford, Oxford OX1 3PU, U.K.*

Yulin Chen − *Department of Physics, Clarendon Laboratory, University of Oxford, Oxford OX1 3PU, U.K.; School of Physical Science and Technology, ShanghaiTech Laboratory for Topological Physics, ShanghaiTech University, Shanghai 201210, China*

Awadhesh Narayan − *Solid State and Structural Chemistry Unit, Indian Institute of Science, Bangalore 560012, India*

Complete contact information is available at: https://pubs.acs.org/10.1021/acsnano.4c01633

Author Contributions

#M.Z., Z.-Y.Z., F.W., and P.L. contributed equally to this work. F.X. conceived the ideas and supervised the overall research. P.L. grew the single crystal. M.Z. and M.O. carried out the magneto-optical measurements. M.Z. and P.L. carried out the transport measurements. M.Z. analyzed the transport and magneto-optical data. Z.-Y.Z. provided the theoretical support of the Hamiltonian. F.W., S.H., Y.C. and Z.L. performed the ARPES measurement. N.B.J. and A.N. performed the DFT calculations. M.Z. and F.X. wrote the paper with help from all other coauthors.

Notes

The authors declare no competing financial interest.

ACKNOWLEDGMENTS

F.X. was supported by the National Natural Science Foundation of China (52225207, 11934005, and 52350001), the Shanghai Pilot Program for Basic Research - FuDan University 21TQ1400100 (21TQ006) and the Shanghai Municipal Science and Technology Major Project (Grant No. 2019SHZDZX01). N.B.J. is supported by the Prime Minister's Research Fellowship (PMRF). A.N. acknowledges support from the startup grant of the Indian Institute of Science (SG/MHRD-19-0001). The infrared measurements were performed at the National High Magnetic Field Laboratory, which is supported by the National Science Foundation Cooperative Agreement No. DMR1644779 and No. DMR2128556 and the State of Florida.

REFERENCES

(1) Soluyanov, A.; Gresch, D.; Wang, Z.; Wu, Q.; Troyer, M.; Dai, X.; Bernevig, B. A. Type-II Weyl Semimetals. *Nature* **2015**, *527*, 495−498.

(2) Li, P.; Wen, Y.; He, X.; Zhang, Q.; Xia, C.; Yu, Z.; Yang, S. A.; Zhu, Z.; Alshareef, H. N.; Zhang, X. Evidence for Topological Type-II Weyl Semimetal WTe_2. *Nat. Commun.* **2017**, *8*, 2150.

(3) Lai, J.; Liu, X.; Ma, J.; Wang, Q.; Zhang, K.; Ren, X.; Liu, Y.; Gu, Q.; Zhuo, X.; Lu, W.; Wu, Y.; Li, Y.; Feng, J.; Zhou, S.; Chen, J.; Sun, D. Anisotropic Broadband Photoresponse of Layered Type-II Weyl Semimetal $MoTe_2$. *Adv. Mater.* **2018**, *30*, 1707152.

(4) Su, B.; Song, Y.; Hou, Y.; Chen, X.; Zhao, J.; Ma, Y.; Yang, Y.; Guo, J.; Luo, J.; Chen, Z. Strong and Tunable Electrical Anisotropy in Type-II Weyl Semimetal Candidate WP_2 with Broken Inversion Symmetry. *Adv. Mater.* **2019**, *31*, 1903498.

(5) Xing, Y.; Shao, Z.; Ge, J.; Luo, J.; Wang, J.; Zhu, Z.; Liu, J.; Wang, Y.; Zhao, Z.; Yan, J.; Mandrus, D.; Yan, B.; Liu, X.; Pan, M.; Wang, J. Surface Superconductivity in The Type II Weyl Semimetal $TaIrTe_4$. *Nat. Sci. Rev.* **2020**, *7* (3), 579−587.

(6) Weng, H.; Liang, Y.; Xu, Q.; Yu, R.; Fang, Z.; Dai, X.; Kawazoe, Y. Topological Node-line Semimetal in Three-Dimensional Graphene Networks. *Phys. Rev. B* **2015**, *92*, 045108.

(7) Yu, R.; Weng, H.; Fang, Z.; Dai, X.; Hu, X. Topological Node-Line Semimetal and Dirac Semimetal State in Antiperovskite Cu_3PdN. *Phys. Rev. Lett.* **2015**, *115*, 036807.

(8) Bian, G.; Chang, T. R.; Sankar, R.; Xu, S.; Zheng, H.; Neupert, T.; Chiu, C. K.; Huang, S. M.; Chang, G.; Belopolski, I.; Sanchez, D. S.; Neupane, M.; Alidoust, N.; Liu, C.; Wang, B.; Lee, C. C.; Jeng, H. T.; Zhang, C.; Yuan, Z.; Jia, S.; et al. Topological Nodal-Line

Fermions in Spin-Orbit Metal $PbTaSe_2$. *Nat. Commun.* **2016**, *7*, 10556.
(9) Wu, Y.; Wang, L.; Mun, E.; Johnson, D. D.; Mou, D.; Huang, L.; Lee, Y.; Bud'ko, S. L.; Canfield, P. C.; Kaminski, A. Dirac Node Arcs in $PtSn_4$. *Nat. Phys.* **2016**, *12*, 667−671.
(10) Li, S.; Guo, Z.; Fu, D.; Pan, X.; Wang, J.; Ran, K.; Bao, S.; Ma, Z.; Cai, Z.; Wang, R.; Yu, R.; Sun, J.; Song, F.; Wen, J. Evidence for a Dirac Nodal-Line Semimetal in $SrAs_3$. *Sci. Bull.* **2018**, *63* (9), 535−541.
(11) Hosen, M. M.; Dhakal, G.; Wang, B.; Poudel, N.; Dimitri, K.; Kabir, F.; Sims, C.; Regmi, S.; Gofryk, K.; Kaczorowski, D.; Bansil, A.; Neupane, M. Experimental Observation of Drumhead Surface States in $SrAs_3$. *Sci. Rep.* **2020**, *10*, 2776.
(12) Schoop, L. M.; Ali, M. N.; Straßer, C.; Topp, A.; Varykhalov, A.; Marchenko, D.; Duppel, V.; Parkin, S. S. P.; Lotsch, B. V.; Ast, C. R. Dirac Cone Protected by Non-Symmorphic Symmetry and Three-Dimensional Dirac Line Node in ZrSiS. *Nat. Commun.* **2016**, *7*, 11696.
(13) Hu, J.; Tang, Z.; Liu, J.; Liu, X.; Zhu, Y.; Graf, D.; Myhro, K.; Tran, S.; Lau, C. N.; Wei, J.; Mao, Z. Evidence of Topological Nodal-Line Fermions in ZrSiSe and ZrSiTe. *Phys. Rev. Lett.* **2016**, *117*, 016602.
(14) Li, S.; Yu, Z.; Liu, Y.; Guan, S.; Wang, S.; Zhang, X.; Yao, Y.; Yang, S. A. Type-II Nodal Loops: Theory and Material Realization. *Phys. Rev. B* **2017**, *96*, 081106.
(15) Chang, T. R.; Pletikosic, I.; Kong, T.; Bian, G.; Huang, A.; Denlinger, J.; Kushwaha, S. K.; Sinkovic, B.; Jeng, H. T.; Valla, T.; Xie, W.; Cava, R. J. Realization of a Type-II Nodal-Line Semimetal in Mg_3Bi_2. *Adv. Sci.* **2019**, *6*, 1800897.
(16) Chen, F. C.; Fei, Y.; Li, S. J.; Wang, Q.; Luo, X.; Yan, J.; Lu, W. J.; Tong, P.; Song, W. H.; Zhu, X. B.; Zhang, L.; Zhou, H. B.; Zheng, F. W.; Zhang, P.; Lichtenstein, A. L.; Katsnelson, M. I.; Yin, Y.; Hao, N.; Sun, Y. P. Temperature-Induced Lifshitz Transition and Possible Excitonic Instability in ZrSiSe. *Phys. Rev. Lett.* **2020**, *124*, 236601.
(17) Pan, H.; Tong, B.; Yu, J.; Wang, J.; Fu, D.; Zhang, S.; Wu, B.; Wan, X.; Zhang, C.; Wang, X.; Song, F. Three-Dimensional Anisotropic Magnetoresistance in the Dirac Node-Line Material ZrSiSe. *Sci. Rep.* **2018**, *8*, 9340.
(18) Gatti, G.; Crepaldi, A.; Puppin, M.; Tancogne-Dejean, N.; Xian, L.; De Giovannini, U.; Roth, S.; Polishchuk, S.; Bugnon, P.; Magrez, A.; Berger, H.; Frassetto, F.; Poletto, L.; Moreschini, L.; Moser, S.; Bostwick, A.; Rotenberg, E.; Rubio, A.; Chergui, M.; Grioni, M. Light-Induced Renormalization of the Dirac Quasiparticles in the Nodal-Line Semimetal ZrSiSe. *Phys. Rev. Lett.* **2020**, *125*, 076401.
(19) Bu, K.; Fei, Y.; Zhang, W.; Zheng, Y.; Wu, J.; Chen, F.; Luo, X.; Sun, Y.; Xu, Q.; Dai, X.; Yin, Y. Visualization of Electronic Topology in ZrSiSe by Scanning Tunneling Microscopy. *Phys. Rev. B* **2018**, *98*, 115127.
(20) Rendy, B.; Hasdeo, E. H. Strain Effects on Band Structure and Dirac Nodal-Line Morphology of ZrSiSe. *J. Appl. Phys.* **2021**, *129*, 014306.
(21) Hosen, M. M.; Dimitri, K.; Belopolski, I.; Maldonado, P.; Sankar, R.; Dhakal, N.; Dhakal, G.; Cole, T.; Oppeneer, P. M.; Kaczorowski, D.; Chou, F.; Hasan, M. Z.; Durakiewicz, T.; Neupane, M. Tunability of the Topological Nodal-Line Semimetal Phase in ZrSiX-Type Materials (X = S, Se, Te). *Phys. Rev. B* **2017**, *95*, 161101.
(22) Rudenko, A. N.; Stepanov, E. A.; Lichtenstein, A. I.; Katsnelson, M. I. Excitonic Instability and Pseudogap Formation in Nodal Line Semimetal ZrSiS. *Phys. Rev. Lett.* **2018**, *120*, 216401.
(23) Song, J.; Wang, J.; Wang, Y.; Zhang, L.; Song, M.; Li, Z.; Cao, L.; Liu, D.; Xiong, Y. Kohler's Rule and Anisotropic Berry-Phase Effect in Nodal-Line Semimetal ZrSiSe. *J. Appl. Phys.* **2022**, *131*, 065106.
(24) Shirer, K. R.; Modic, K. A.; Zimmerling, T.; Bachmann, M. D.; König, M.; Moll, P. J. W.; Schoop, L.; Mackenzie, A. P. Out-of-Plane Transport in ZrSiS and ZrSiSe Microstructures. *APL Mater.* **2019**, *7*, 101116.
(25) Kirby, R. J.; Ferrenti, A.; Weinberg, C.; Klemenz, S.; Oudah, M.; Lei, S.; Weber, C. P.; Fausti, D.; Scholes, G. D.; Schoop, L. M. Transient Drude Response Dominates Near-Infrared Pump−Probe Reflectivity in Nodal-Line Semimetals ZrSiS and ZrSiSe. *J. Phys. Chem. Lett.* **2020**, *11*, 6105−6111.
(26) Dong, E.; Liu, R.; Niu, S.; Luo, X.; Hu, K.; Tian, H.; Liu, B.; Li, X.; Li, Y.; Zhu, X.; Li, Q.; Liu, B. Pressure-Induced Electronic and Structural Transition in Nodal-Line Semimetal ZrSiSe. *Inorg. Chem.* **2021**, *60*, 11140−11146.
(27) Shao, Y.; Rudenko, A. N.; Hu, J.; Sun, Z.; Zhu, Y.; Moon, S.; Millis, A. J.; Yuan, S.; Lichtenstein, A. I.; Smirnov, D.; Mao, Z. Q.; Katsnelson, M. I.; Basov, D. N. Electronic Correlations in Nodal-Line Semimetals. *Nat. Phys.* **2020**, *16*, 636−641.
(28) Sankar, R.; Peramaiyan, G.; Muthuselvam, I. P.; Butler, C. J.; Dimitri, K.; Neupane, M.; Rao, G. N.; Lin, M.; Chou, F. C. Crystal Growth of Dirac Semimetal ZrSiS with High Magnetoresistance and Mobility. *Sci. Rep.* **2017**, *7*, 40603.
(29) Aroyo, M. I.; Kirov, A.; Capillas, C.; Perez-Mato, J. M.; Wondratschek, H. Bilbao Crystallographic Server. II. Representations of Crystallographic Point Groups and Space Groups. *Acta Crystallogr.* **2006**, *62*, 115−128.
(30) Shao, Y.; Sun, Z.; Wang, Y.; Xu, C.; Sankar, R.; Breindel, A. J.; Cao, C.; Fogler, M. M.; Millis, A. J.; Chou, F.; Li, Z.; Timusk, T.; Maple, M. B.; Basov, D. N. Optical Signatures of Dirac Nodal Lines in $NbAs_2$. *Proc. Natl. Acad. Sci. U.S.A.* **2019**, *116*, 1168−1173.
(31) Abergel, D. S. L.; Apalkov, V.; Berashevich, J.; Ziegler, K.; Chakraborty, T. Properties of Graphene: a Theoretical Perspective. *Adv. Phys.* **2010**, *59*, 261−481.
(32) Orlita, M.; Basko, D. M.; Zholudev, M. S.; Teppe, F.; Knap, W.; Gavrilenko, V. I.; Mikhailov, N. N.; Dvoretskii, S. A.; Neugebauer, P.; Faugeras, C.; Barra, A.; Martinez, G.; Potemski, M. Observation of three-dimensional massless Kane fermions in a zinc-blende crystal. *Nat. Phys.* **2014**, *10*, 233.
(33) Sadowski, M. L.; Martinez, G.; Potemski, M.; Berger, C.; de Heer, W. A. Magnetospectroscopy of Epitaxial Few-Layer Graphene. *Solid State Commun.* **2007**, *143*, 123−125.
(34) Aoki, H.; Dresselhaus, M. S. *Physics of Graphene*; Springer Science & Business Media, 2013; pp 124−126.
(35) Abergel, D. S. L.; Fal'ko, V. I. Optical and Magneto-Optical Far-Infrared Properties of Bilayer Graphene. *Phys. Rev. B* **2007**, *75*, 155430.
(36) Giannozzi, P.; Baroni, S.; Bonini, N.; Calandra, M.; Car, R.; Cavazzoni, C.; Ceresoli, D.; Chiarotti, G. L.; Cococcioni, M.; Dabo, I.; Dal Corso, A.; de Gironcoli, S.; Fabris, S.; Fratesi, G.; Gebauer, R.; Gerstmann, U.; Gougoussis, C.; Kokalj, A.; Lazzeri, M.; Martin-Samos, L.; et al. QUANTUM ESPRESSO: a Modular and Open-Source Software Project for Quantum Simulations of Materials. *Journal of Physics Condensed Matter* **2009**, *21*, 395502.
(37) Giannozzi, P.; Andreussi, O.; Brumme, T.; Bunau, O.; Buongiorno Nardelli, M.; Calandra, M.; Car, R.; Cavazzoni, C.; Ceresoli, D.; Cococcioni, M.; Colonna, N.; Carnimeo, I.; Dal Corso, A.; de Gironcoli, S.; Delugas, P.; DiStasio Jr, R. A.; Ferretti, A.; Floris, A.; Fratesi, G.; Fugallo, G.; Gebauer, R.; et al. Advanced Capabilities for Materials Modelling with Quantum ESPRESSO. *Journal of Physics Condensed Matter* **2017**, *29*, 465901.
(38) Grimme, S. Semiempirical GGA-type density functional constructed with a long-range dispersion correction. *J. Comput. Chem.* **2006**, *27* (15), 1787−1799.
(39) Perdew, J. P.; Burke, K.; Ernzerhof, M. Generalized Gradient Approximation Made Simple. *Phys. Rev. lett.* **1996**, *77*, 3865.

https://doi.org/10.1021/acsnano.4c01633
ACS Nano 2024, 18, 16684−16691